CHARACTERIZATION OF PORE STRUCTURES ON THE LOWER SILURIAN MARINE SHALE GAS PLAY

A Thesis

Presented to

the Faculty of the Department of Petroleum Engineering

University of Houston

In partial fulfillment of requirements for the degree of

Master of Science

in Petroleum Engineering

by

Yang Jiang

May 2014

CHARACTERIZATION OF PORE STRUCTURES ON THE LOWER SILURIAN MARINE SHALE GAS PLAY

_____

Yang Jiang

Approved:

_____

Chair of the Committee
Guan Qin, Associate Professor,
Department of Petroleum Engineering

Committee Members:

_____

W. John Lee, Professor,
Department of Petroleum Engineering

_____

Suresh K. Khator, Associate Dean,
Cullen College of Engineering

_____

Thomas K. Holley, Professor and
Director of Department in Petroleum
Engineering

ACKNOWLEDGEMENTS

I would like to express my sincere gratitude to my advisor, Dr. Guan Qin, for his continued guidance in my research and life, for his enthusiasm, patience and immense knowledge, also for his love that treat his students as family members.

Besides my advisor, I would like to thank the rest of my thesis committee: Prof. Holly and Prof. John Lee, for their encouragement, insightful comments. In particular, I am grateful for having the opportunity to work with Dr. Holly in Petrophysics course.

My sincere thanks also goes to Prof. Jun Yao, Prof. Aifen Li, and Ying Gao from China University of Petroleum (East), for providing me guidance and the license of the digital core modelling software.

I would like to thank my friends in our research group for the stimulating discussions in our office. Also I thank my friends in University of Wyoming and China University of Petroleum, for all the fun and time we spent together.

Last but not the least, I would like to thank my family: my mom and dad, for their endless love and support. Also I want to thank my uncle and aunt for helping me find the felling of home in Houston. I want to thank my girlfriend Juan Juan for her love and understanding in the last four years.

CHARACTERIZATION OF PORE STRUCTURES ON THE LOWER SILURIAN MARINE SHALE GAS PLAY

An Abstract of a Thesis

Presented to

the Faculty of the Department of Petroleum Engineering

University of Houston

In partial fulfillment of requirements for the degree of

Master of Science

in Petroleum Engineering

by

Yang Jiang

May 2014

ABSTRACT

Gas shales are different from conventional reservoir as the strata are both source rock and reservoir rock for gas, and no structural or stratigraphic traps are needed to retain the gas. The recent advances in horizontal drilling and hydraulic fracturing stimulations have made vast shale gas resource commercially viable. However, due to the complex nature of gas storage, the quantification of shale gas reservoirs has been proven extremely challenging. Shale formation is usually extremely tight and the majority of the pores are nano-pores in which the diameters of the pores are in the range of several nanometers to tenth of nanometers.

In this research, we propose to perform the numerical sensitivity study of nanopore structures on fluid flow. The proposed research will involve: Generation of 3-dimensional digital core of nano-pore structures based on the Scanning Electron Microscope (SEM) images of real core samples that are collected from the Longmaxi Formation - Lower Silurian Marine Shale Gas Play in Southern China. The results indicate that digital core is an efficient way to characterize the micropores structure of the shale formation parameters.

DEDICATION

To my parents

TABLE OF CONTENTS

LIST OF FIGURES

LIST OF TABLES

CHAPTER 1:Introduction

1.1 Statement of Problem

The supply of natural gas has changed dramatically as the unconventional natural gas has been developed commercially since last decade. Unconventional gas resources including: shale gas, coal bed methane and tight gas, in which, shale gas is the most rapidly growing unconventional gas resources especially in the United States. From the energy projections of the United States released on April 2013 by Energy Information Administration (EIA, 2013), the U.S. natural gas production will increase from 23 trillion cubic feet (TCF) in 2011 to 33 TCF in 2040 with a 44% increase and most of the increase is due to the production of shale gas, as shown in Figure 1-1.

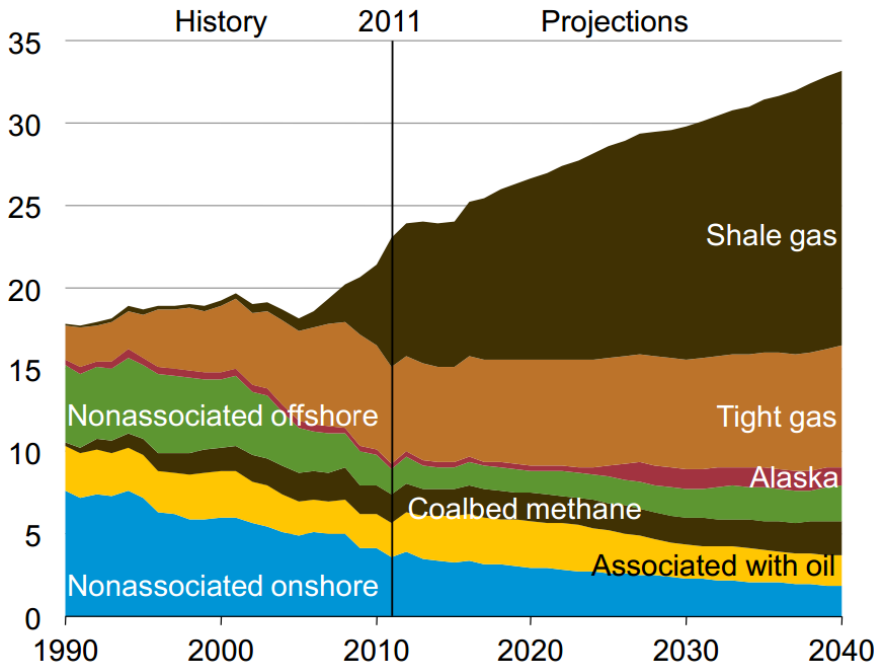

Figure 1-1 U.S. Dry Natural Gas Production by Source (TCF), 1990-2040

The successful recovery of shale gas in the United States is fueled by two major technologies, one is horizontal drilling and the other is hydraulic fracturing (Osborn et al., 2011). These technologies were introduced to shale gas industry in the early 1990s which helped the United States enter a "shale revolution."

Following the success of shale gas development in the U.S., China has started to develop its resources in a large scale also a rapid fashion. China has an advantage in shale gas production that it holds the world's largest potential reserves of shale gas (EIA 2013). The 1337 trillion cubic feet (TCF) technically recoverable shale gas reserves is mainly located in 4 areas (EIA, 2012), which are Northern Areas, Tarim basin, Qaidam/ Qiantang basin and Southern Areas (Figure 1-2). The Southeastern Sichuan Basin is considered as the most prolific shale gas play, in which the main target layer is the lower Silurian Longmaxi Formation. Evidence has shown that the lower part of Silurian shale is a marine shale gas play, and several exploratory wells have been drilled in the Longmaxi Formation (Wei, 2013).

However, the highly potential Longmaxi formation still faces many challenges for developing (Nick Feast, 2013). First, the permeability of the Longmaxi formation is too low to produce at commercial rates without treatment such as hydraulic fracturing. But, hydraulic fracturing is expensive to perform and requires experts to design complex fracturing design, which made hydraulic fracturing inconvenient to this area. Second, horizontal wells are difficult to drill, because the formation has high structural complexity,

it is difficult to control the drilling bit to stay in the preferred zone. Third, the ultra-low matrix porosity ranges from 3% to 10% combined with a small drainage area, more wells are needed which will raise the cost.

Figure 1-2 Major Unconventional Natural Gas Resources in China

The shale gas reservoirs still face a multitude of challenges in reservoir characterization and production aspect, mainly because they are different from conventional reservoirs. The shale strata are both source rock and reservoir rock for shale gas, and no stratigraphic or structural traps are needed to retain gas, due to the permeability of the shale formation is extremely low. The pore structure of shale formation is very complex which have been proved by various studies (Zhang, 2012). A significant amount of shale gas is stored in the complex submicron pore structures; however, the mechanisms of shale gas storage and flow in porous media are not well understood yet. So,

understanding of porosity, permeability, pore size distribution and pore structure is crucial for effective reservoir management and production prediction.

It is well-know, the macroscopic properties of the reservoir, such as permeability, capillary pressure, depends on its microstructure of solid composition and physical properties of the fluid in the void space. In other words, the microstructure of the formation, the rock and fluid properties are the fundamental theory of the flow in porous media, which the macroscopic properties are the appearance of the microscopic properties. Therefore, to achieve the goal of significantly enhance oil recovery, the theoretical research and technological development cannot just stay at the macro level. In-depth study of internal porous media in micro level should be emphasized. Only in this way, we can have a fundamental understanding of the contact between microscopic with the macroscopic, which will lead us to the right direction of the EOR and the proper technique to develop shale reservoir.

In order to have a better understanding of the microstructure in the Longmaxi formation, petrophysical experiments are conducted to measure the petrophysical properties. Also, the scanning electron microscope is used to visualize the pore types existed in this formation. Models both in 2 dimensions and 3 dimensions are constructed and validated, which will provide a better knowledge of flow mechanism and storage space of the shale formation.

1.2 Objective of the Study

The objectives of the proposed research are:

To provide high resolution images of the nanopores by using SEM and characterize all observable pore types in the Longmaxi samples with special emphasis on the predominant nanopore types, which can help to understand the gas storage mechanism in the Silurian marine shale reservoir.

To measure petrophysical parameters, porosity, permeability and pore-size distribution, of the Longmaxi formation. The obtained data is used to characterize the Lower Silurian Marine shale gas play.

To develop, 2D pore-scale binary image, which are required as input data for numerical simulation. Also, a method to transfer SEM image to binary image is introduced, two sets of Matlab code are developed for solution.

To build 3D digital core, with the utilization of Markov Chain Monte Carlo method, based on the SEM data. And data, such as porosity, permeability and pore-size distribution, are calculated by 3DQ19 Lattice Boltzmann model. Then compare the simulation results of the 3D digital core with the experiment data, in order to check whether the Markov Chain Monte Carlo method can be applied to build a digital core in shale formation.

1.3 Thesis Outline

This thesis is divided into seven chapters. After a brief introduction of this study. Chapter 2 covers the experimental studies, which include petrophysical study and

visualization study. Detailed procedures are introduced to measure petrophysical parameters and identify different pore types. Chapter 3 presented a method to change the SEM image to binary image, which is used for creating a finite element mesh in nano-scale. The Markov Chain Monte Carlo method is employed to reconstruct a 3D digital core of this shale formation. Parameters are solved by 3DQ19 Lattice Boltzmann model. Presentation and discussion of the results obtained are explained in Chapter 4. In the end, conclusions made during this study and suggestions for future work is provided in the final chapter.

CHAPTER 2:Experimental Study

As we mentioned before, the shale formations has ultra-low porosity and permeability which made the mechanisms of shale gas storage and flow complicated. Research has shown that the main parameter controls the deliverability of gas shales are porosity and permeability (Sondergeld et al., 2010). So, emphasis is placed on the determination of microstructure in the shale formation, which is also the main topic of this study.

In this section, we conducted experiments like Scanning Electron Microscope, gas expansion experiment, pulse decay experiment and nitrogen adsorption experiment, on cores from the Longmaxi shale formation. Parameters, such as permeability, porosity and pore size distribution, are obtained by utilizing these experiments. The microstructure and different pore types are also visualized. For our previous studies on the Longmaxi formation (Wei, 2013), 12 samples range in depth from 6279ft to 6385ft were examined in detail.

2.1 Virtualization Experiment

For this study, 4 samples from the Longmaxi marine shale were analyzed using the SEM visualization experiment. After a detailed SEM study of numerous specimens, several types of pores were recognized and detailed discussion is shown in Chapter 4.

2.1.1 **Scanning Electron Microscope Experiment**

A scanning electron microscope (SEM) is a type of vital equipment to produce images of a sample in micro and nanometer scale. The SEM can be used to obtain detailed information of the surface or near-surface region of a specimen with a focused beam of electrons. A Scanning electron microscope can be split into three parts- an electron optical column, a vacuum system and electronics (Figure 2-1).

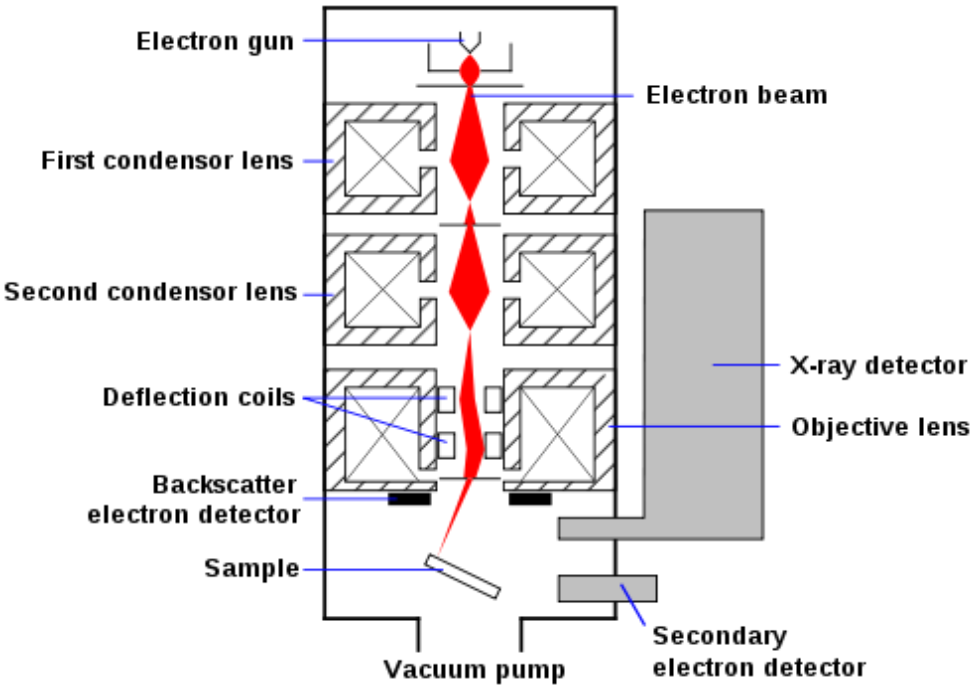

Figure 2-1 Scheme of a Scanning Electron Microscope

The electron gun inside the electron optical column produces an electron beam that is focused into the rectangular target on the specimen as small as 1 nm. The electron beam reached and interact with the specimen that various signals (mostly secondary electron signal) can be created and measured in computer memory. This obtained information is then shown as image data. The magnification is defined as the ratio of the size of the

displayed image to the size of the area scanned, which means by reducing the size of the area scanned on the specimen the magnification increases. Because the image in modern SEMs is created and stored in a computer, it can be readily transferred for other uses. The specimen used for SEM experiment have to be clean, dry, vacuum-compatible and electrically conductive. The quality of the image in a SEM depends on the orientation and distance of the specimen from the final lens. The movements of the sample are controlled by a computer which can be turned in X, Y and Z directions as required (Hall, 1953).

Recent interest by petroleum engineers to better understand shale reservoir has led to an increased utilizing SEM technology in the industry. The scanning electron microscopy is used to study different aspects of the composition of shale samples at very high resolution. It can provide different modes and techniques for acquiring high resolution images for Longmaxi shale formation (Figure 2-2).

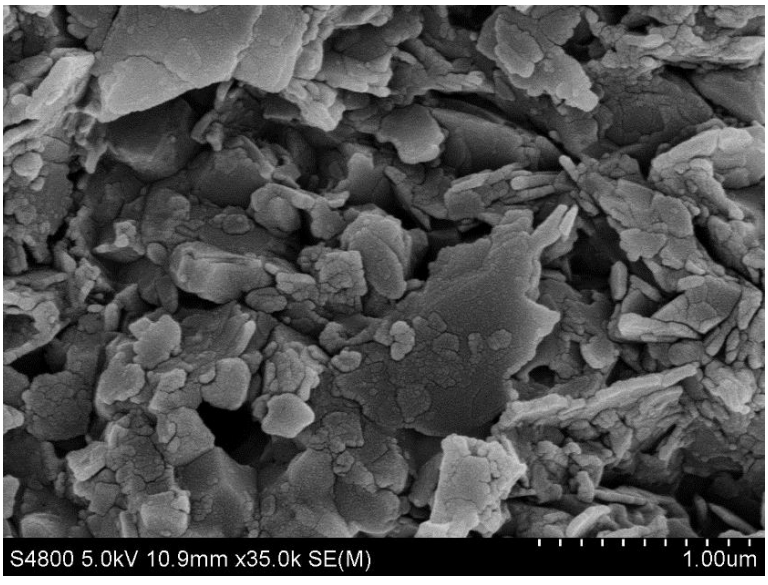

Figure 2-2 Scanning Electron Microscope Image from Longmaxi Formation

2.2 Petrophysical Parameter Analysis

2.2.1 Porosity

Porosity ϕ is defined as the fraction of the total bulk volume that is taken up by the pore space. The void volume is usually determined by a clean and dried core by one of the following methods (Ashraf, 1994):

- Saturation with liquid;
- Extraction of gas content
- Gas compression and expansion in the pore space by Boyle's Law

For porosity measurements, the method we used is the helium gas expansion experiment. The gas expansion experiment relies on Boyle's law. The reason we choose helium as the experiment gas is because the molecular diameter of helium is really small. The pore in the shale formation is usually nanometer pores, such small molecular diameter can get into these pores easily. Also, for safety consideration, helium is relatively stable, which it doesn't react with other material. The scheme of helium gas expansion experiment is shown below (Figure 2-3).

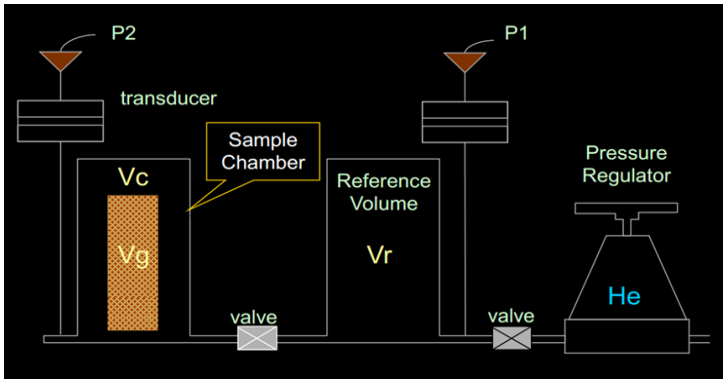

Figure 2-3 Scheme of Helium Gas Expansion Experiment

In this experiment, both of the containers is vacuumed in advance. Rock is sealed in sample container with known volume V_g at pressure 0 and this container is attached by a valve to the reference container with volume V_r and pressure P_1. When the valve is opened, two containers are connected; the pressure will reach an equilibrium value P_2. The bulk volume V_b is then measured by Archimedes method. Porosity can be calculated by the following equation:

The porosity ϕ is defined as

$$\phi = \frac{V_{pore}}{V_{bulk}},$$

where

$$P_1 V_r = P_2 (V_r + V_c - V_g) \quad \text{and}$$

$$V_{bulk} = V_{grain} + V_{pore}$$

2.2.2 **Permeability**

The permeability is the ability for a formation to conduct fluid. It is one of the most fundamental properties of any reservoir rock, which is required for production modeling (Sakhaee-Pour, 2012). There are still technical challenges of measurement of low permeability to water; in this study we conducted the transient pulse decay experiment for more accurate analysis.

For conventional reservoirs, permeability is measured by constant-pressure steady-state-flow based on Darcy's Law. However, the constant pressure method requires a lot of

time for shale, due to the extremely tight and ultra-low permeability. The method used for this study is the transient pulse decay method, which it reduce the measurement time by changing the boundary condition and core size. The boundary changed from constant pressure to the pressure vary with time. The measurement procedure is shown as following:

First the Pulse Decay Permeameter (Figure 2-4) saturates the sample with nitrogen to a set pore pressure, and then transmits a differential pressure pulse through the sample. As the pressure transient propagates though the sample, the computer records the pressure difference across the sample, the downstream pressure, and time. Permeability is calculated from a linear regression performed on the pressure time data and the results stored to a data file.

Then the apparent gas permeability can be calculated based on the method original proposed by Brace. The pulse is a small step change of differential pore fluid pressure imposed between two reservoirs connected at the ends of the sample. When a pressure pulse ΔP is applied, the differential pressure ΔP (t) decays exponentially as a function of time t

$$\Delta \mathrm{P}(\mathrm{t}) = \Delta P_0 e^{-mt},$$

where, t is testing time and m is a decay time constant. Then the plot, $\ln\Delta \mathrm{P}(t)$ vs. time t, is plotted with a slope of m. The permeability k can be determined by the equation

$$\mathrm{k} = \mathrm{m}\mu \mathrm{Z}\left(\frac{\mathrm{L}}{\mathrm{A}}\right) \times \left[\frac{V_1 V_2}{V_1 + V_2}\right],$$

where

V_1 and V_2 are the upstream and downstream reservoir volumes,

L= length of the measured sample,

A= cross-section area,

μ =Nitrogen viscosity, and

Z= compressibility of Nitrogen.

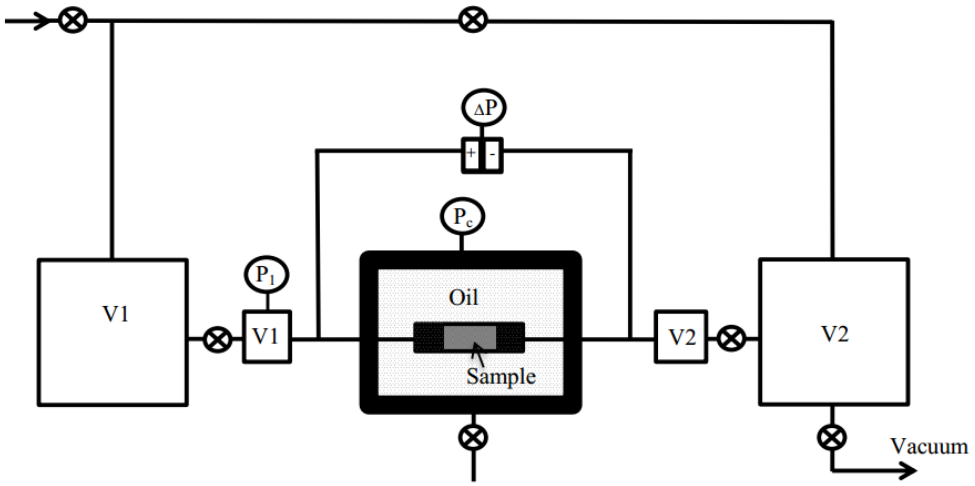

Figure 2-4 Schematic Diagram of the Pulse Decay Permeameter

2.2.3 **Pore Size Distribution**

The pore size distribution is a quantitative measure of the range of pore sizes for a given sample. A soil's pore size distribution combined with the porosity characterize the pore space. The pore diameter of shales varies significantly, which the pore sizes are usually specified by an effective radius of the pore body.

Pore size distribution in a porous media is often determined by mercury injection experiment. However, ultra-high pressure, around 60000psi is required for mercury fill full

with the pores in the shale formation (Nimmo, 2004). This kind of high pressure may destroy the pore structure in the shale formation, which may lead to inaccurate measurement results. The method applied in this study is the nitrogen adsorption experiment. The pore-size distribution can be obtained from the gas adsorption and desorption isotherms which subjected to adsorption and capillary condensation in the pores (Seaton, 1989). The gas often used is nitrogen, which desorbed and condensed at the temperature of liquid Nitrogen. It becomes a standard tool for determination of the pore size distribution for shale.

In the nitrogen adsorption experiment, the core samples need to be crushed and mixed thoroughly in a sample tube. Then the sample is mixed with liquid nitrogen, which the tube is measured in an instrument. The pressure is applied in the instrument and the nitrogen characteristic is measured with computer. The nitrogen isothermal is shown in Figure 2-5, where the relative pressure p/p0 is the ratio of partial pressure of the adsorbed substance to saturated vapor pressure of the adsorbed gas.

Based on the data of nitrogen adsorption isothermal, BJH method is used to calculate the pore size distribution of each sample. The BJH method (Barrett et al., 1951) is developed by Barrett, Joyner and Halenda in 1951, based on the assumption that pores have a cylindrical shape and that pore radius is equal to the sum of the Kelvin radius and the thickness of the film adsorbed on the pore wall. BJH method uses a modified Kelvin

equation which predicts the pressure at which adsorptive will spontaneously condense in a cylindrical pore of a given size.

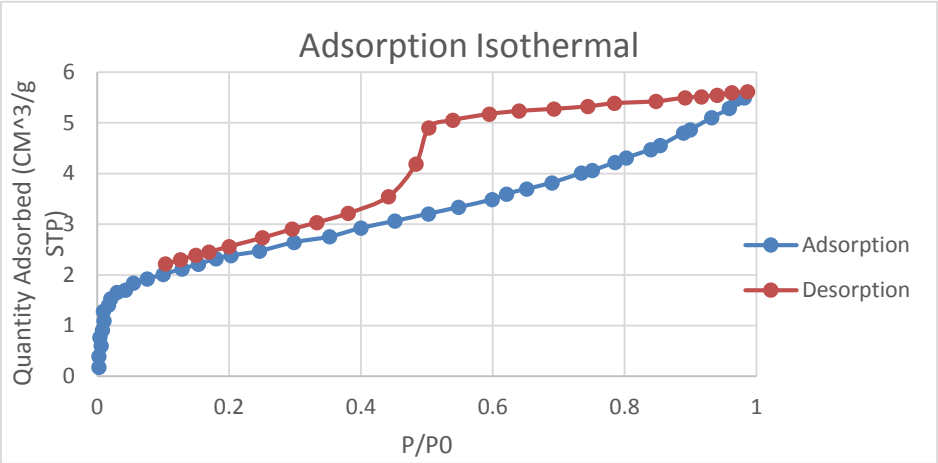

Figure 2-5 Adsorption Isothermal of Core from Longmaxi Formation

CHAPTER 3:Construction of Digital Cores

The laboratory measurements of the petrophysical parameters have been obtained and shown in chapter 2. However, these measurements do not provide microstructural parameters for this shale formation (Driskill et al., 2013). In order to investigating and estimating the physical and fluid flow properties of the porous media, digital core has been introduced in recent years. Digital core is a novel approach that high resolution images of the rock sample are obtained and processed, which is built by the information provided by the high resolution images. The created digital cores are used for numerical simulation with an emphasis on the fluid flow in the pore scale (Grader et al., 2010).

Digital core modeling techniques (Yao et al., 2013) can be divided into two categories: physical experiments method and numerical reconstruction method. Physical experiments method is acquiring the three-dimensional core structure data, digital core, using high-precision instrument, which include: CT and FIB/SEM.

A focused ion beam (FIB) experiment is almost identical to a SEM experiment, but the beam used has changed from electrons to a beam of ions. The FIB is also used as a micro- and nano-machining tool. In a process called sputtering, the ion beam directly mills the surface of the specimen, and the milling can be controlled within nanometer scale. When FIB is combined with SEM, the electron and ion beams intersect at a 52 °angle at a coincident point near the sample surface, allowing immediate, high resolution SEM

imaging of the FIB-milled surface. The combined FIB/SEM tomography becomes a powerful tool for three dimensional imaging of core samples.

The physical method is costly and need high requirements for the equipment, which lead to the difficulties for industry uses. Furthermore, such methods are also limited by the resolution and the image scale, because high resolution image large image scale cannot be achieved at the same time.

Numerical reconstruction (Wang, 2012) refers to a digital core is reconstructed by numerical calculation based on a small number of 2D thin section images. Current common numerical reconstruction methods are: Gaussian simulation method, process simulation method, simulated annealing, multi-point statistical method and Markov chain Monte Carlo method.

Understanding the 3D pore network model is the foundation for multiphase flow in porous media studies, which the microscopic pore network is able to reproduce the complex pore structure and pores distribution. The simulation of flow in pores media can not only reduce the cost and time of physical experiment, but also obtain the data that are difficult to measure in the laboratory, which has a significant influence on enhancing oil recovery. In this study, we applied the numerical method to construct 3 dimensional digital core for the Lower Silurian marine shale formation. Detailed modelling procedure and methodology is discussed in this chapter.

3.1 Binary image

In order to distinguish pore with rock solid, we need to change the grayscale image obtained for SEM experiment to a binary image. A binary image is a digital image that has only two possible values for each pixel. Typically the two colors used for a binary image are black and white though any two colors can be used. In a binary system, the binary image is a data only contain 0 and 1, i.e., 0 or 1 represent for pore or solid respectively. However, the edge of the rock matrix pores are very vague, detailed image segmentation is needed. In order to clearly distinguish the pore and solid in the SEM gray-scale image, a reasonable threshold value need to be find, which the image pixels are divided into two groups – black and white. At present, common image binarization methods include: Otsu method, Global threshold method, in which, Otsu method is mostly used and reliable.

3.1.1 Otsu Method

Otsu's method (Otsu, 1979) is an image segmentation method which an optimal threshold is selected to classify the pixels in a gray scale image into two categories. In Otsu's method the threshold that minimizes the intra-class variance (the variance within the class) need to be found. In Otsu's method, the pixels of a L gray levels picture can be represented as [1, 2…,L]. The total number of pixels is denoted by N and the number of pixels at level I is denoted by n_i, which

$$N = n_1 + n_2 .$$

The gray-level histogram is normalized and regarded as a probability distribution:

$$p_i = n_i / \mathrm{N} \quad \text{and}$$

$$p_i \geq 0, \sum_{i=1}^{L} p_i = 1.$$

In image segmentation, the pixels are classified in to two classes C_0 and C_1(pore and rock) by a threshold at level k; C_0 denotes pixels with levels [1,…k], and C_1 denotes pixels with levels [k+1, …., L]. The probabilities of class occurrence and the class mean levels, respectively, are given by

$$\omega_0 = \Pr(C_0) = \sum_{i=1}^{k} p_i = \omega(k) \quad \text{and}$$

$$\omega_1 = \Pr(C_1) = \sum_{i=k+1}^{L} p_i = 1 - \omega(k).$$

The probability of class mean levels is given by:

$$\mu_0 = \sum_{i=1}^{k} i \Pr(i|C_0) = \sum_{i=1}^{k} \frac{ip_i}{\omega_0} = \mu(k) / \omega(k) \quad \text{and}$$

$$\mu_1 = \sum_{i=k+1}^{L} i \Pr(i|C_1) = \sum_{i=k+1}^{L} \frac{ip_i}{\omega_1} = \frac{\mu_T - \mu(k)}{1 - \omega(k)},$$

where

$$\omega(k) = \sum_{i=1}^{k} p_i,$$

and

$$\mu(k) = \sum_{i=1}^{k} ip_i.$$

The total mean level of the original picture is

$$\mu_T = \mu(L) = \sum_{i=1}^{L} i p_i .$$

$$\omega_0 \mu_0 + \omega_1 \mu_1 = \mu_T , \text{ and}$$

$$\omega_0 + \omega_1 = 1 .$$

The class variance is

$$\sigma_0^2 = \sum_{i=1}^{k} (i - \mu_0)^2 \Pr(i|C_0) = \sum_{i=1}^{k} i - \mu_0 \ ^2 p_i \quad \omega_0 \text{ and}$$

$$\sigma_1^2 = \sum_{i=k+1}^{L} (i - \mu_1)^2 \Pr(i|C_1) = \sum_{i=k+1}^{L} (i - \mu_1)^2 \, p_i / \omega_1 .$$

The within-class variance is defined as

$$\sigma_W^2 = \omega_0 \sigma_0^2 + \omega_1 \sigma_1^2 ,$$

$$\sigma_B^2 = \omega_0 (\mu_0 - \mu_T)^2 + \omega_1 (\mu_1 - \mu_T)^2 = \omega_0 \omega_1 (\mu_1 - \mu_T)^2 ,$$

and the total variance is

$$\sigma_T^2 = \sum_{i=1}^{L} (i - \mu_0)^2 \, p_i .$$

Then the problem is simplified to an optimization problem to search for a threshold k that maximizes in the previous equations.

The optimal threshold k is

$$\sigma_B^2(k) = \max_{1 \le k < L} \left| \sigma_B^2(k) \right. .$$

Matlab provides a high-level language and development tools that let us quickly change the grayscale image to binary image. The Matlab (2012) code listing shown in Fig. illustrates how this is accomplished in the code.

```
function imagBW = otsu(imag)
imag = imag(:, :, 1);

[counts, x] = imhist(imag);  % counts are the histogram. x is the intensity
level.
GradeI = length(x);    % the resolusion of the intensity. i.e. 256 for
uint8.
varB = zeros(GradeI, 1);  % Between-class Variance of binarized image.

prob = counts ./ sum(counts);  % Probability distribution
meanT = 0;  % Total mean level of the picture
for i = 0 : (GradeI-1)
   meanT = meanT + i * prob(i+1);
end
varT = ((x-meanT).^2)' * prob;
% Initialization
w0 = prob(1);   % Probability of the first class
miuK = 0;   % First-order cumulative moments of the histogram up to the
kth level.
varB(1) = 0;
% Between-class variance calculation
for i = 1 : (GradeI-1)
   w0 = w0 + prob(i+1);
   miuK = miuK + i * prob(i+1);
   if (w0 == 0) || (w0 == 1)
      varB(i+1) = 0;
   else
      varB(i+1) = (meanT * w0 - miuK) .^ 2 / (w0 * (1-w0));
   end
end

maxvar = max(varB);
em = maxvar / varT  % Effective measure
index = find(varB == maxvar);
index = mean(index);
th = (index-1)/(GradeI-1)
imagBW = im2bw(imag, th);
% thOTSU = graythresh(imag)
% imagBWO = im2bw(imag, thOTSU);
```

3.1.2 **Niblack's Method**

The Niblack's method (Niblack, 1985) is a binarization method based on the calculation of the local mean m and the standard deviations. The threshold is decided by the formula:

$$T_{Niblack} = m + k \times s$$

$$T_{Niblack} = m + k\sqrt{\frac{1}{NP}\sum(p_i - m)^2} = m + k\sqrt{\frac{\sum p_i^2}{NP} - m^2} = m + k\sqrt{B},$$

where NP is the pixel number of the original image,

m is the mean value for pixels, and k is fixed to -0.2 in this case. The advantage of Niblack method is that it always identifies the text regions correctly as foreground.

The Matlab code is shown below:

```
tic;
k = -0.2;  % the first manual parameter
b = 80;   % the second manual parameter, about the width of the square
neighborhood
choice = 1; % 1 for pixel-to-pixel computation, 2 for pixel averaging
within the square neighborhood for fast computation.
imag = imag( :, :, 1);
[Hei, Wid] = size(imag);

imag = padarray(imag, [b b], 'symmetric', 'both');  % Pad image array
Hei_pad = Hei + 2 * b;
Wid_pad = Wid + 2 * b;
imagBW = false(Hei_pad, Wid_pad);
switch choice
   case 1
      for i = 1+b : Hei+b
         for j = 1+b : Wid+b
            upR = i-floor(b/2-1/2);
            dnR = i+floor(b/2);
```

```
            lfC = j-floor(b/2-1/2);
            rtC = j+floor(b/2);
            m_ij = mean(mean(imag(upR : dnR, lfC : rtC)));
            sigma_squared = double(imag(upR : dnR, lfC : rtC)) - m_ij;
            sigma_squared = mean(mean(sigma_squared .^2));
            sigma = sqrt(sigma_squared);
            th_ij = m_ij + k * sigma;
            if double(imag(i,j)) > th_ij
               imagBW(i,j) = 1;
            end
         end
      end
   case 2
      for i = 1+b : b : Hei+b
         for j = 1+b : b : Wid+b
            upR =  i-floor(b/2-1/2);
            dnR =  i+floor(b/2);
            lfC =  j-floor(b/2-1/2);
            rtC =  j+floor(b/2);
            m_ij = mean(mean(imag(upR : dnR, lfC : rtC)));
            sigma_squared  =  double(imag(upR  :  dnR,  lfC  :  rtC))  -
repmat(m_ij, (dnR-upR+1), (rtC-lfC+1));
            sigma_squared = sigma_squared .^ 2;
            sigma_squared = mean(mean(sigma_squared));
            sigma = sqrt(sigma_squared);
            th_ij = m_ij + k * sigma;
            imagBW(upR : dnR, lfC : rtC) = double(imag(upR : dnR, lfC :
rtC)) > th_ij;
         end
      end
   otherwise
      display('Wrong Choice!');
end
imagBW = imagBW(1+b : Hei+b, 1+b : Wid+b);
% figure, imshow(imagBW), title('Binarized Image');
toc;
```

Based on these image segmentation methods, the grayscale image obtained from the SEM (Figure 3-1) can be transferred into binary image (Figure 3-2). From Figure 3-2the

pore body and gas flow channel can be separated very clearly, and the binary image itself is a data only include 0 and 1. In this case, 0 is pore and 1 is rock matrix.

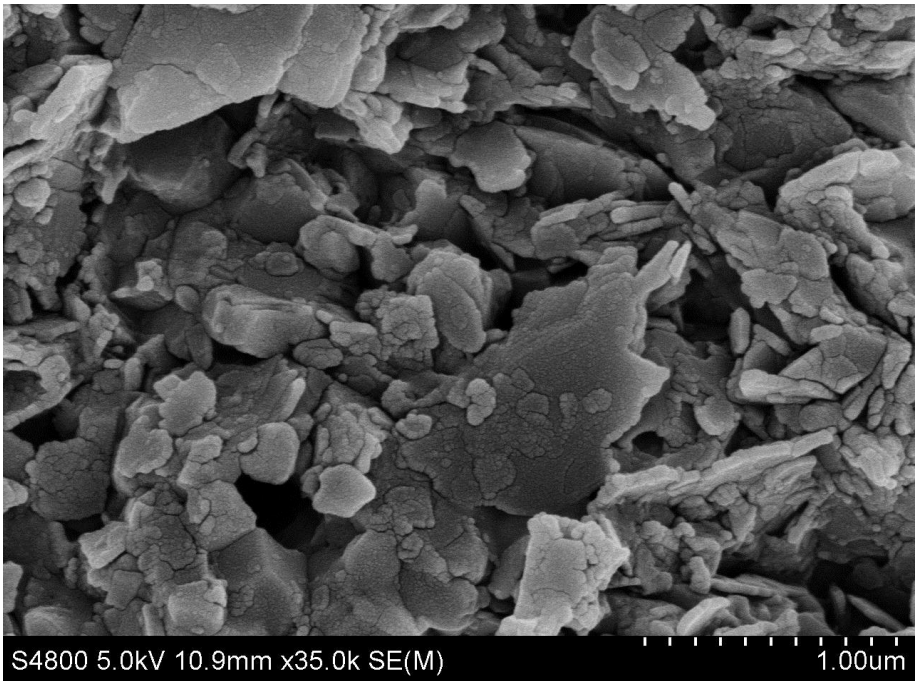

Figure 3-1 SEM Image of Pore-structures on the Longmaxi Formation

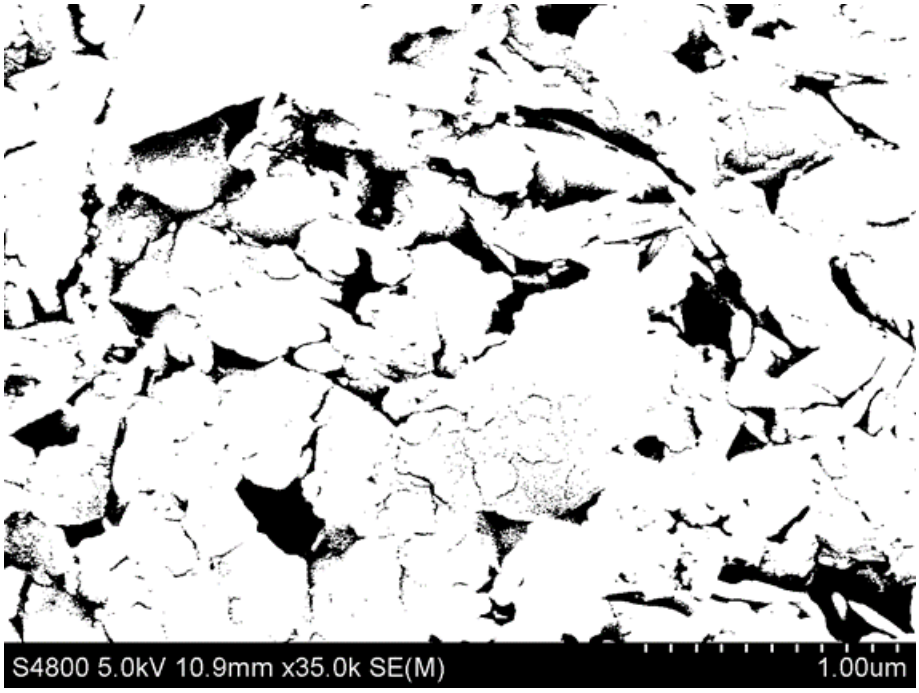

Figure 3-2 Binary Image Transferred from the SEM Image

3.2 Markov Chain Monte Carlo

In order to understand the Markov Chain Monte Carlo, Markov Chain and Monte Carlo simulation should be understood separately. Markov Chain is a mathematical system is controlled by a transition matrix (or transition probability) that the next state is only depend on the previous state. It is a stochastic process with the Markov property, which refers to a sequence of random variables have this kind of properties. The Monte Carlo simulation is a computational algorithms that rely on repeated random sampling to obtain numerical results, by which the probability distribution function can be found by Monte Carlo simulation.

The Markov Chain Monte Carlo (MCMC) methods is a simulation approach that uses the previous sample values to randomly generate the next sample value, which generating a Markov chain. The generated Markov Chain is used for Monte Carlo simulation. The transition probabilities between sample values are only a function of the most recent sample value. The method provide an efficient way to simulate a sequence of random draws form very complicated stochastic models.

The Markov Random Fields is multi-dimensional Markov Chain, which is widely used in image processing research. The MRF theory uses only a small number of local conditions to predict global features based on given data, which means, it only considers the interaction and relations of a few local neighbors data and some other geometrical data to generate the overall features of the image. In building the digital rock the global feature

is the porous media (Wu, et al., 2006). The scanning algorithm has been applied to update the image a row of pixels at a time, which lead to a much faster convergence. The software used to create digital cores in this study is developed by China University of Petroleum. Detailed procedure is shown below in the following chapter.

In this study, we use voxels as sites to build the Markov Chain model. Suppose we have a finite lattice of n voxels(X1, …,Xn), which X has the value, 0 or 1 for pore and solid respectively. To build a 3D digital core, we need to know the probability distribution function for all the voxels. However, the 3 dimensional image is hard to acquire and the 3D sample space is too large to have a probability distribution function. So, we need to use the Markov Random Field models, which assuming the state of any voxel is depend only on the states of a small number of neighboring sites, to build this model, and then use the Monte Carlo simulation to find the probability distribution of the matrix.

As we stated, the Markov Random Fields can be treated as a multi-dimensional version of Markov Chain. Here, some assumptions are made to this model in priority:

- The structure of the shale formation is spastically correlated;
- For a particular site s, Λ-s represents all sites other than s. The neighborhood of s, Ns is

$$p(x_s \mid x(\Lambda_{-s})) \approx p(x_s \mid x(N_s));$$

- Use only past voxel information to avoid iteration;
- The voxel (i, j , k) at the intersection of row I, column j and layer k is

VLMN = {(l,m,n) : 0 < l ≤L rows, 0<m ≤M columns, 0<n≤N layers}.

After these assumptions are made, the SEM image is used as input data to build the model, because the shale formation structure is spatially correlated. The distributions in equation is difficult to simulate and take a long time to reach convergence, which limiting the application in high-dimensional cases. By using only past voxel information can save iteration time.

For any (i,j,k) ∈VLMN, the joint probability function is

$$\mathrm{p}\left(\mathrm{x}\left(V_{ijk}\right)\right)=\prod_{l=0}^{i}\prod_{m=0}^{j}\prod_{n=0}^{k}p(x_{lmn}\left|x_{l-1,mn},x_{l,m-1,n},x_{l,m,n-1}\right.)\,.$$

The conditional probability for each voxel is

$$\mathrm{p}\left(x_{ijk}\left|\left\{x_{lmn}:(l,m,n)\neq(i,j,k)\right\}\right.\right)=p(x_{ijk}\left|\left\{x_{lmn}:(l,m,n)=N(i,j,k)\right\}\right.).$$

For example, a 19-neighbourhood with its 18 neighbors is

$$N_{19}(ijk)=\begin{bmatrix}(i-1,j,k) & (i,j-1,k) & (i,j,k-1)\\ (i+1,j,k) & (i,j+1,k) & (i,j,k+1)\\ (i,j-1,k+1) & (i-1,j,k+1) & (i-1,j+1,k)\\ (i,j+1,k-1) & (i+1,j,k-1) & (i+1,j-1,k)\\ (i,j+1,k+1) & (i+1,j,k+1) & (i+1,j+1,k)\\ (i,j-1,k-1) & (i-1,j,k-1) & (i-1,j-1,k)\end{bmatrix}$$

However, this 19-neighbourhood model involves past voxel, if the model is built from bottom to the upward. So, a 15-neighbourhood model is used instead (Wu, 2006). This model updating two voxels (i,j,k) and (i,j+1,k) simultaneously based on the information of the 13 neighborhoods, which can reduce the simulation time. The 15-neighbourhood with its 13 neighbors is

$$N_{15}(ijk; i, j+1, k)\begin{bmatrix} (i-2, j, k-1) & (i-2, j+1, k-1) & (i-1, j, k-1) \\ (i-1, j+1, k-1) & (i, j-1, k-1) & (i, j, k-1) \\ (i, j+1, k-1) & (i-2, j, k) & (i-2, j+1, k) \\ (i-1, j-1, k) & (i-1, j, k) & (i-1, j+1, k) \\ (i, j-1, k) & & \end{bmatrix}.$$

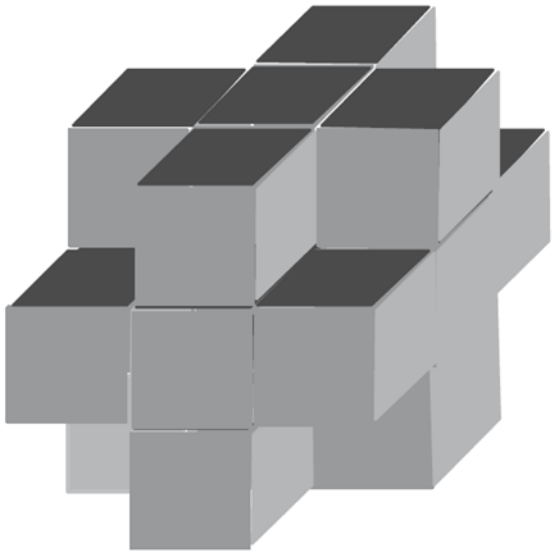

Figure 3-3 19-Neighborhood Model (Wu, 2006)

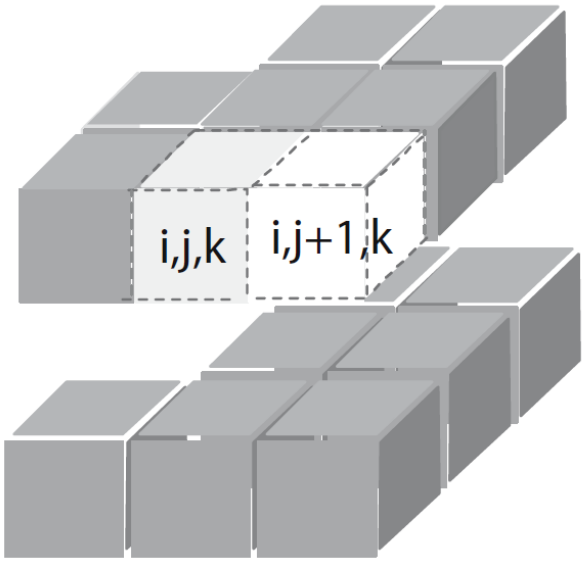

Figure 3-4 15-Neighbourhood Model (Wu, 2006)

The problem becomes to find out the transition probability to build 3D Markov Chain, which in this case is the digital core. First, the transition probabilities between the voids and solids in 2D SEM binary image should be found out. To find out the 2D transition probability, we applied 5- and 6-neighborhoods models (Figure 3-5 and Figure 3-6). The transition probabilities are

$$p(x_{ij} \,|\, x(N_5(ij))) \quad \text{and}$$

$$p(x_{i,j+1} \,|\, x(N_6(i, j+1))).$$

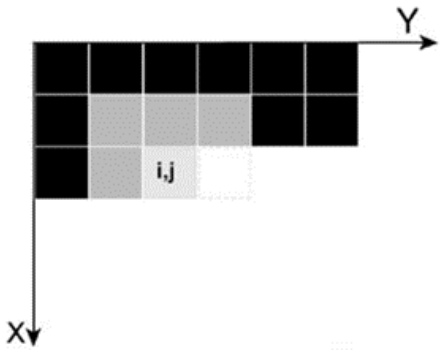

Figure 3-5 5-Neighborhood Model

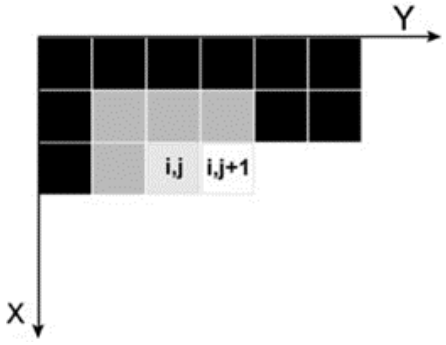

Figure 3-6 6-Neighborhood Model

After the 2D transition probability is obtained, the 2D model is combined to a 3D transition probability with 11- and 12-neigborhoods model, which the transition probability are:

For 11-neigborhoods

$$p(x_{ijk}\,|\,x(N_{11}(ijk))) = \left\{ p(x_{ijk}\,|\,x(N_{i,5}(ijk))) + p(x_{ijk}\,|\,x(N_{j,6}(ijk))) + p(x_{ijk}\,|\,x(N_{k,5}(ijk))) \right\};$$

For 12-neigborhoods model

$$p(x_{i,j+1,k}\,|\,x(N_{12}(i,j+1,k))) = \begin{Bmatrix} p(x_{i,j+1,k}\,|\,x(N_{i,6}(i,j+1,k))) + p(x_{i,j+1,k}\,|\,x(N_{j,6}(i,j+1,k))) \\ + p(x_{i,j+1,k}\,|\,x(N_{k,6}(i,j+1,k))) \end{Bmatrix}.$$

In the absence of the three-dimensional information, we use three perpendicular binary images to construct a three-dimensional Markov Chain (Figure 3-7 Reconstruction by Numerical Method).

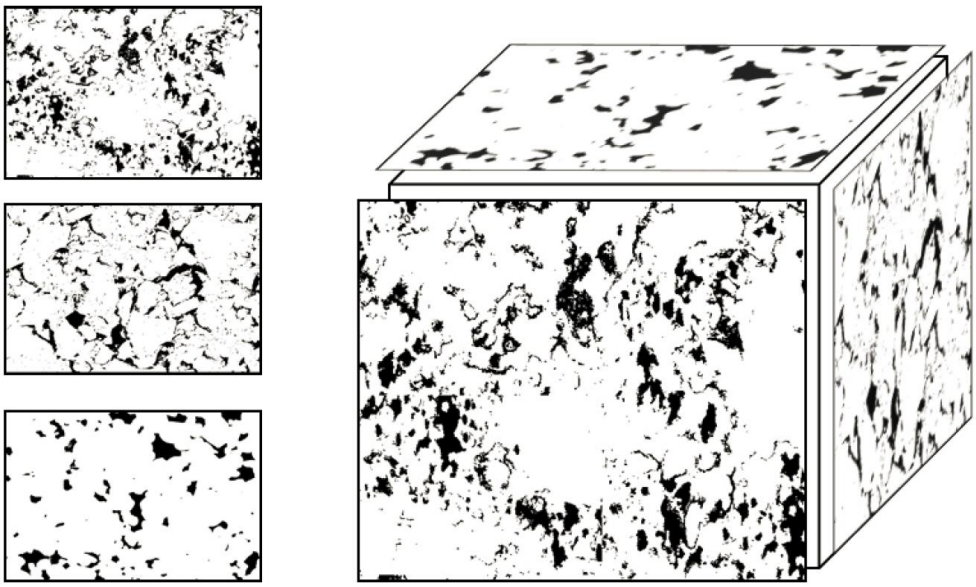

Figure 3-7 Reconstruction by Numerical Method

The concrete steps to build three-dimensional digital core based on Markov Chain Monte Carlo are as follows:

1. Simulate one dimensional voxel chain, using the conditional probability of the porosity of the porosity obtained from SEM binary image (Figure).

2. Simulate the first row of voxels in the y direction of the first layer. The first row of the second voxels is simulated using two neighbors. Then from the third voxels, the voxels begins to simulate by three neighbors. The conditional probability is deduced from the information in xy plane.

3. Simulate all the voxels of first layer in the x direction, in order to construct the first layer of the digital core. In one scan, the row by row of the first layer in two-dimensional is constructed, which 3 and 4 neighborhood on the edge, 5 and 6 neighborhood used with in the frame.

4. The first row of the second layer is formed similar to step 2, but we use a vertical 4 neighborhood voxel followed by 6 neighbor hoods in the same plane. The inside voxels are simulated by the full 3D 15 neighborhood described below.

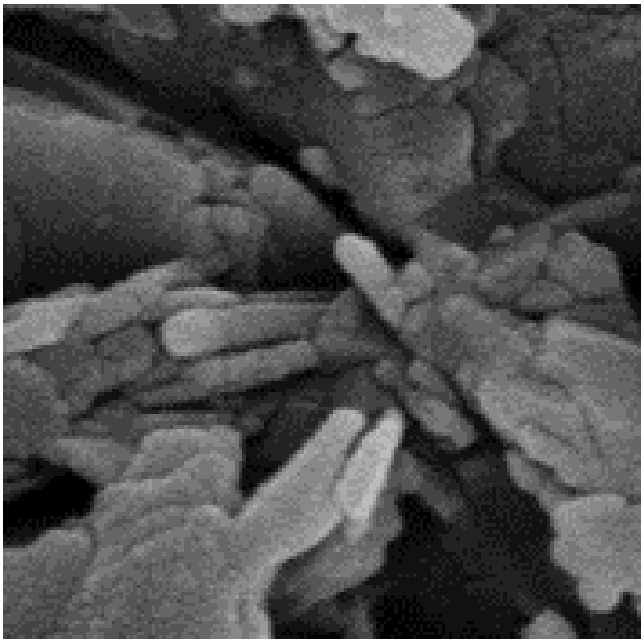

Figure 3-8 SEM Image Used for Reconstruction of Digital Cores

Figure 3-9 Binary Image Used for Reconstruction of Digital Cores

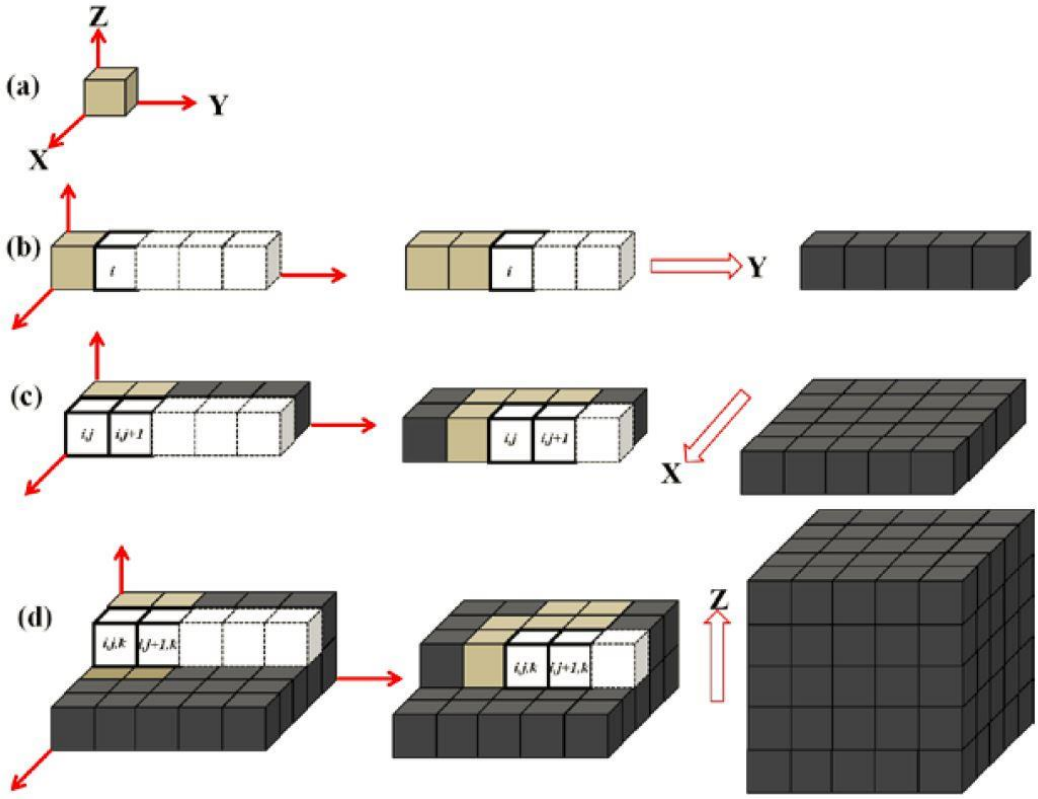

Figure 3-10 Procedures of Reconstruction 3D Markov Chain

Thus, Markov Chain Monte Carlo method can be used to construct 3D digital core based on the high resolution 2D SEM image. This method directly and quickly builds the pore characteristics of micro-digital core from three directions. The modelling method is fast and accurate.

3.3 Lattice Boltzmann

Lattice Boltzmann method (LBM) is a class of computational fluid dynamics techniques based on kinetic theory (Ning, 2011). It differs from the conventional computational fluid dynamics techniques which based on the Navier-Stokes equations. The N-S equations are shown to be the results of collective behavior of many macroscopic particles. Instead of solving the N-S equations numerically, the LBM models the particles distribution function for fluids. The LBM has several advantages over the conventional CFD techniques including simplicity of the algorithm, ability to introduce complex fluid physics, ease of implementation on parallel clusters, etc. In this study, we applied the LBM to evaluate the permeability of the digital cores.

The Boltzmann equation describes the statistical distributions of particles in fluids. It is an integral-differential equation for the single particle distribution function $f(\vec{x},\vec{\varepsilon},t)$, which describes the probability of finding a particle in a volume and with a velocity in the range. The form is

$$\frac{\partial f}{\partial t}+\vec{\xi}\cdot\nabla f = C(f),$$

where C is the collision operator that contains very complicated integral terms, and $\vec{\xi}$ is the particle velocity. A simplification of this collision integral C(f) is the Bhatnagar-Gross-Krook (BGK) approximation,

$$C(f) \approx -\frac{1}{\tau_0}(f - f^{eq}) .$$

In BGK model (Qian et al., 1992), the most widely used is DdQm model (d is detentions and m is discrete particle velocities) which is proposed by Qian et al.. It is a basic notation to represent lattice velocity structure. In this study, we use D3Q19 model to calculate the absolute permeability of the core that particles move in 19 directions and every voxel containing 19 particle distribution functions. A set of velocity vectors are described as

$$\vec{e}_i = \begin{cases} (0,0,0) & i = 0 \\ (\pm 1,0,0),(0,\pm 1,0),(0,0,\pm 1) & i = 1,...,6 \\ (\pm 1,\pm 1,0),(\pm 1,0,\pm 1),(0,\pm 1,\pm 1) & i = 7,...,18 \end{cases} .$$

The evolution equation is

$$f_i(x + e_i \Delta t) = f_i(x,t) - \frac{1}{\tau}(f_i(x,t) - f_i^{eq}(x,t) .$$

The discrete values of the equilibrium function is defined

$$f_i^{eq} = t_\sigma \rho \left[1 + 3\frac{e_i u}{c^2} + 4.5\frac{(e_i u)^2}{c^4} - 1.5\frac{u^2}{c^2} \right] .$$

The macroscopic flow variables are

$$\rho = \sum_i f_i(x,t) \quad \text{and}$$

$$\rho u = \sum_i f_i(x,t) e_i .$$

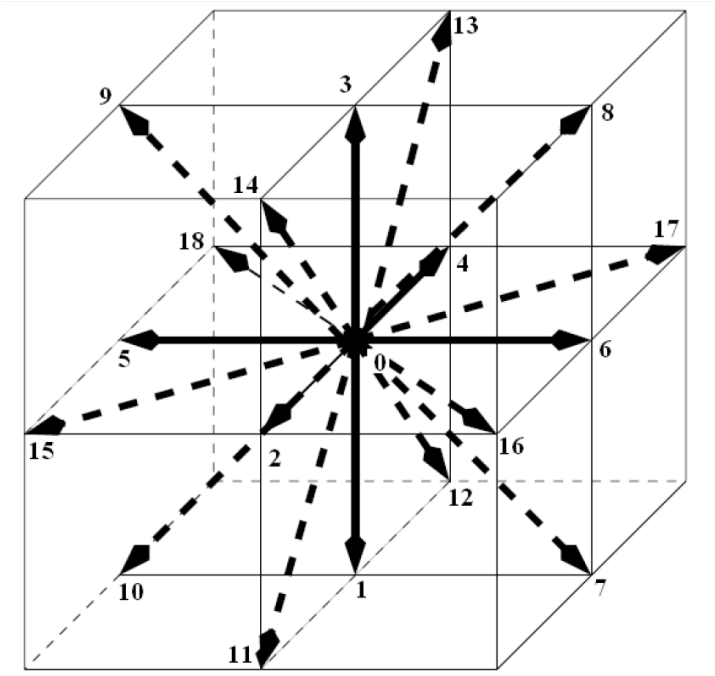

Figure 3-11 D3Q19 Lattice Boltzmann Model

In the permeability calculation, the fluid flow in the core is set, and it is surrounded by a layer of rock. In order to ensure the second order accuracy, we use the curve boundary condition between pore and matrix. The inlet and outlet we apply a certain pressure gradient Δp. The results for the created digital cores are shown in the result and discussion section.

CHAPTER 4:Result and discussion

This chapter discusses the results obtained from laboratory experiments, scanning electron microscope experiments, and numerical experiments. This chapter is divided into three parts. The first section discusses the pore network and variety of pore types exists in the Longmaxi formation, which are observed based on the SEM experiment. The second part of the chapter compares the petrophysical parameters, such as porosity, permeability and pore size distribution, between experiment results and digital core simulation results. The last part of this chapter shows some preliminary results and future work of this study.

4.1 SEM Microstructure Virtualization

Based on the observation from SEM images with different level of magnifications, kerogen (organic matter) can be identified based on its unique morphologies, and the pore radius can be calibrated. Also, various types of porosity are observed as shown in figures below, which can help us to understand the different accumulation mechanisms within different types of porosity.

For this study, samples from the Longmaxi marine shale were analyzed using the SEM visualization experiment. After a detailed SEM study of numerous specimens, several types of pores were recognized and separated into two groups based on the pore size: micropores and nanopores (Table 4-1) (Loucks, 2009). Based on our observation to these samples, the most abundant pore type in the Longmaxi shale formation is nanopores.

Table 4-1 Pore Classification by Diameter

Nanopore	≤ 75μm
Micropore	≥ 75 nm

4.1.1 **Micropores**

Micropores are found in microfossils, fragmentary or pyrite framboids. Pores associated with the cavities of fossils are present. However, most of the micropores are associated with diagenetic minerals, for example pyrite (Figure 4-1), this evidence indicates that the Longmaxi formation went through an anoxic diagenetic process. The pyrite framboids can provide small voids for gas storage. The pore bodies in the pyrite framboids changes with the framboids size. The framboids with smaller size (2–10 um in size) usually contain pores range in size from 0.05 to 1 um , whereas the larger framboids shows pores ranging from 1 to 5 nm in diameter. Pore shapes are generally polyhedral with straight margins. As a group, micropores are relatively rare in Longmaxi shale except for those in pyrite framboids.

4.1.1 **Nanopores**

In the nanoscale range, even a single crystalline solid has intrinsic void spaces, which the crystalline may only compose atoms or ions. So, pores in nanoscale are classified into intraparticle pores and interparticle pores. Interparticle nanopores have been observed and those pores are usually developed at the margins of grains (Figure 4-2). Interparticle pores

associated with grain boundaries tend to be relatively large with diameters of hundreds of nanometers and are more common in this formation.

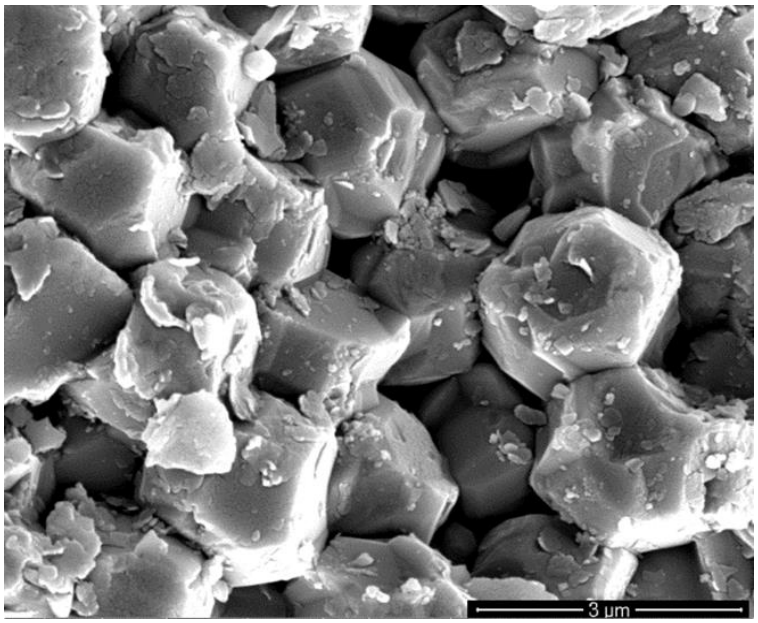

Figure 4-1 Pores Inside the Pyrite Framboids

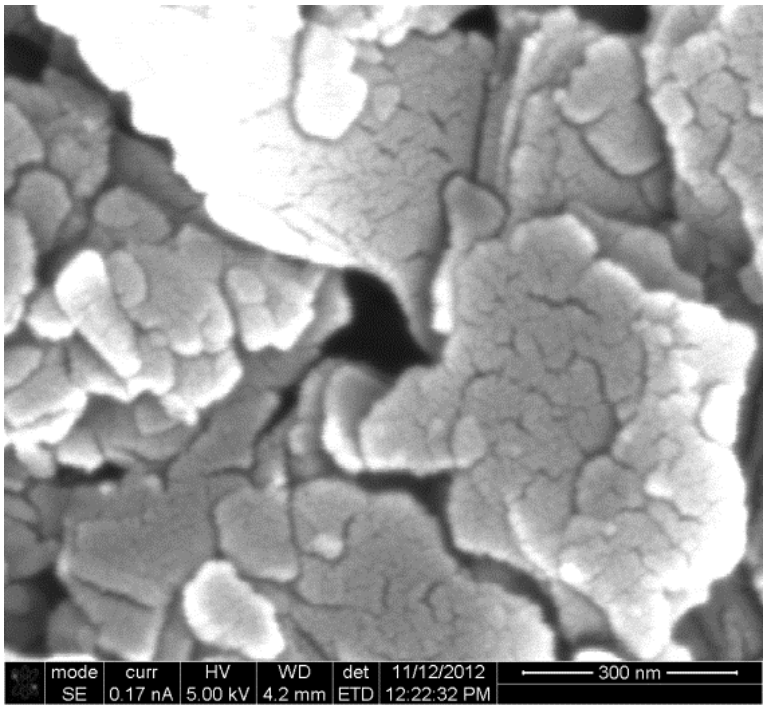

Figure 4-2 Interparticle Pores in the Longmaxi Formation

Intraparticle nanopores, which means pores within grains, are often found in the organic matter which is the most widespread and numerous pore types in the Longmaxi Shale. The pore shapes are vary from nearly spherical to irregularly polygonal, with slightly irregular ellipsoids being the most common shape.

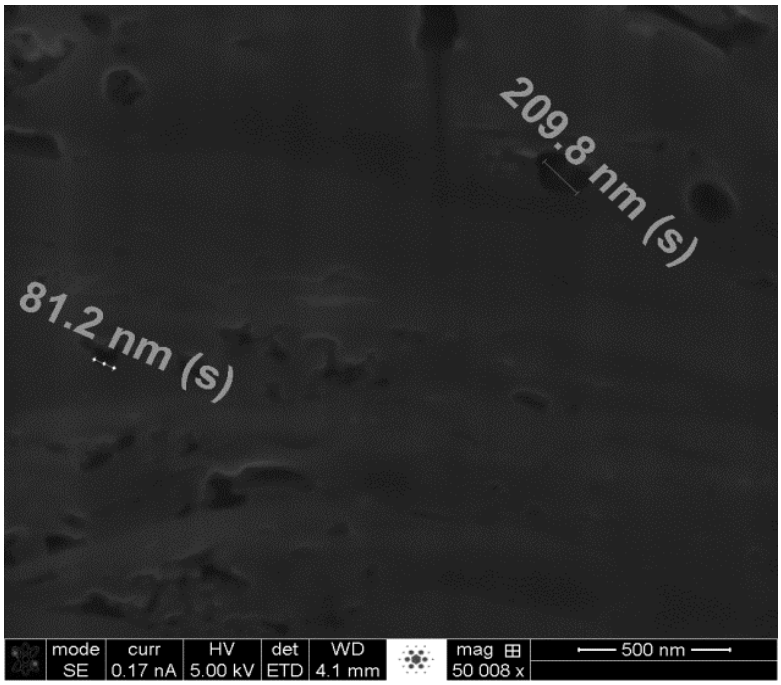

Figure 4-3 Pores Associated with Organic Matter

Based on the SEM images above, various types of porosity are observed, which includes intergranular pores, intragranular pores, pores around and within pyrite, and pores in organics matters. These observed pores in the formation will provide storage space and transport channel for shale gas.

4.2 Data Comparison

From the petrophysical experiment, three parameters are measured by the experiment mentioned in chapter 2, which are the permeability, porosity and pore-size distribution. By

helium gas expansion experiment, the porosity of four samples from the Longmaxi formation is shown in Table 4-2 with an average porosity 2.75%. The permeability is measured by transient pulse decay experiment, with an average permeability 2.025 micro-Darcy (Table 4-3). The experiment results shows that the Longmaxi formation is really tight and have ultra-low permeability and porosity.

Table 4-2 Porosity of 4 Core Samples from Longmaxi Formation

Core No.	Sample 1	Sample 2	Sample 3	Sample 4	Average
Porosity (%)	2.6	2.9	3	2.5	2.75

Table 4-3 Permeability of 4 Core Samples from Longmaxi Formation

Core No.	Sample 1	Sample 2	Sample 3	Sample 4	Average
Permeability(uD)	2.4	2.1	2	1.7	2.025

The pore-size distribution (Figure 4-4) is obtained from the nitrogen adsorption experiment shows that the pores in the Longmaxi formation is mainly nano pores, which also verified the observation results from the SEM experiment.

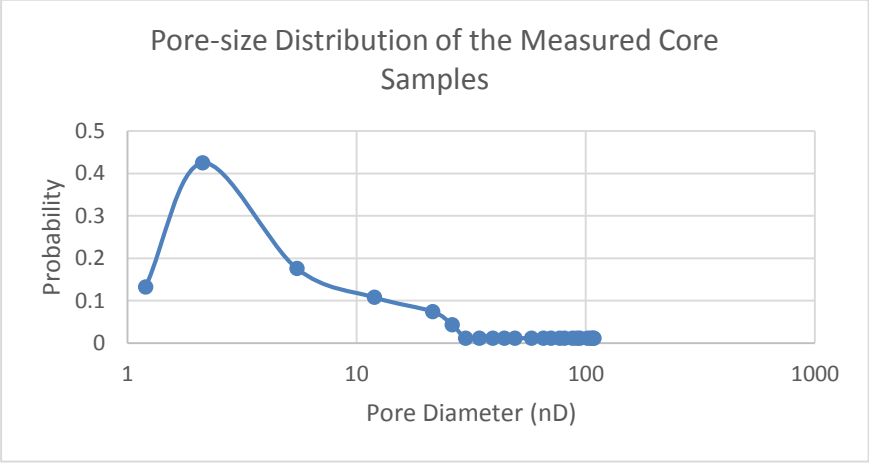

Figure 4-4 Pore-size Distribution from the Nitrogen Adsorption Experiment

After applied the 3D Markov Chain Monte Carlo modelling approach to the Longmaxi shale formation, 5 digital cores were obtained ()we compared the petrophysical data obtain from digital core with the experiment data. The compared results are summarized in table, which can illustrate the capability of the modelling approach in shale formation.

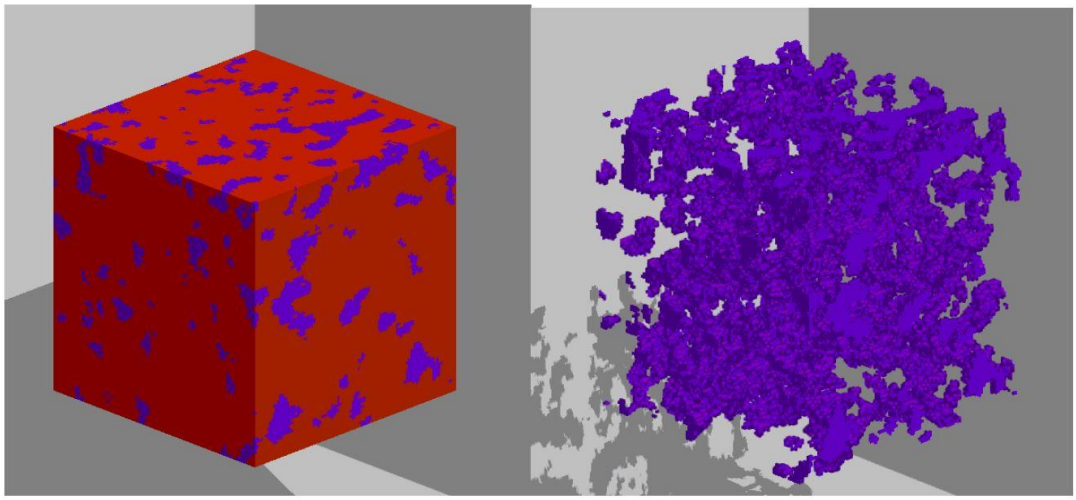

Figure 4-5 Digital Structure and Pore Structure of Sample 1

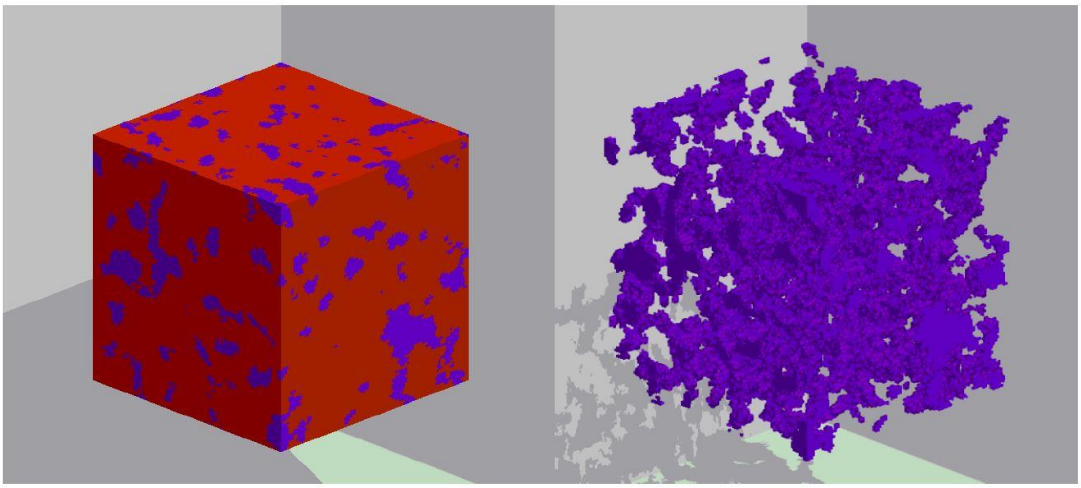

Figure 4-6 Digital Structure and Pore Structure of Sample 2

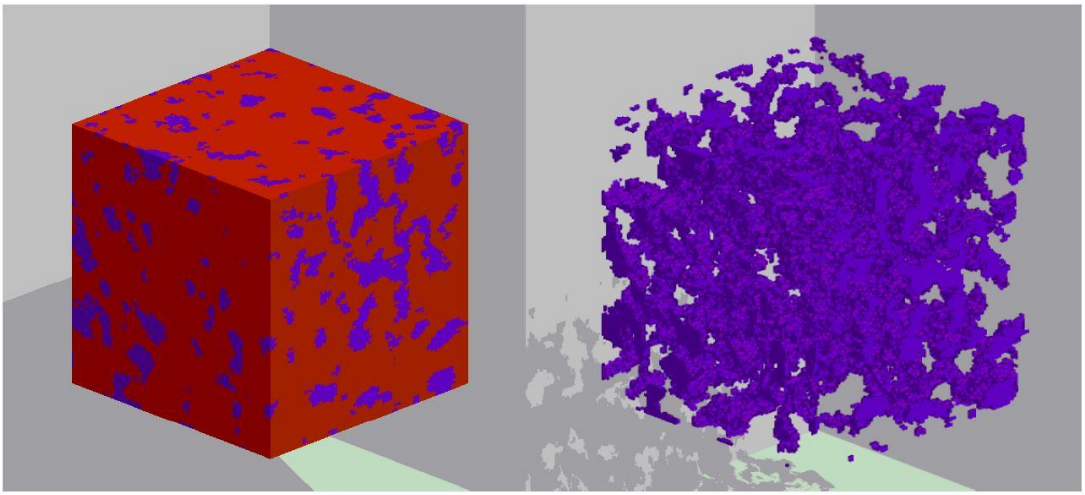

Figure 4-7 Digital Structure and Pore Structure of Sample 3

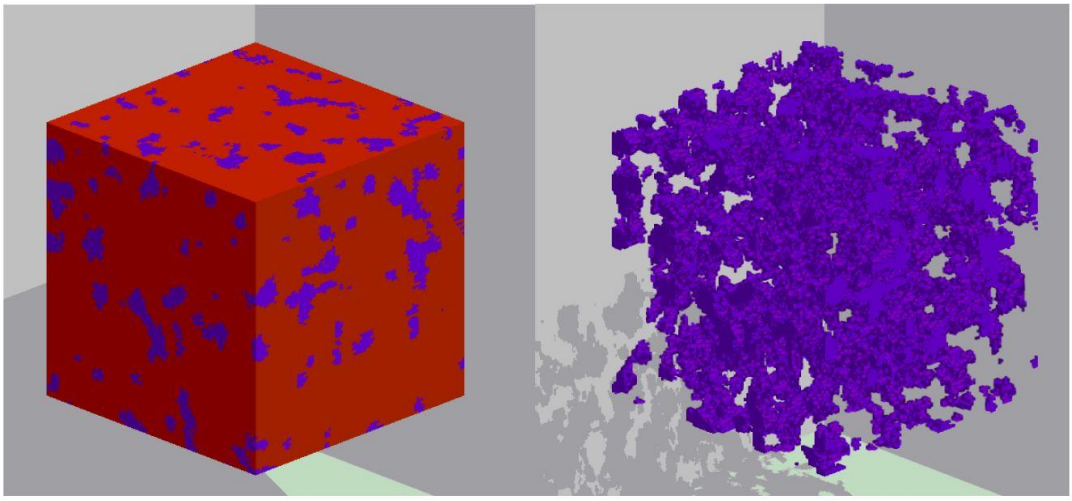

Figure 4-8 Digital Structure and Pore Structure of Sample 4

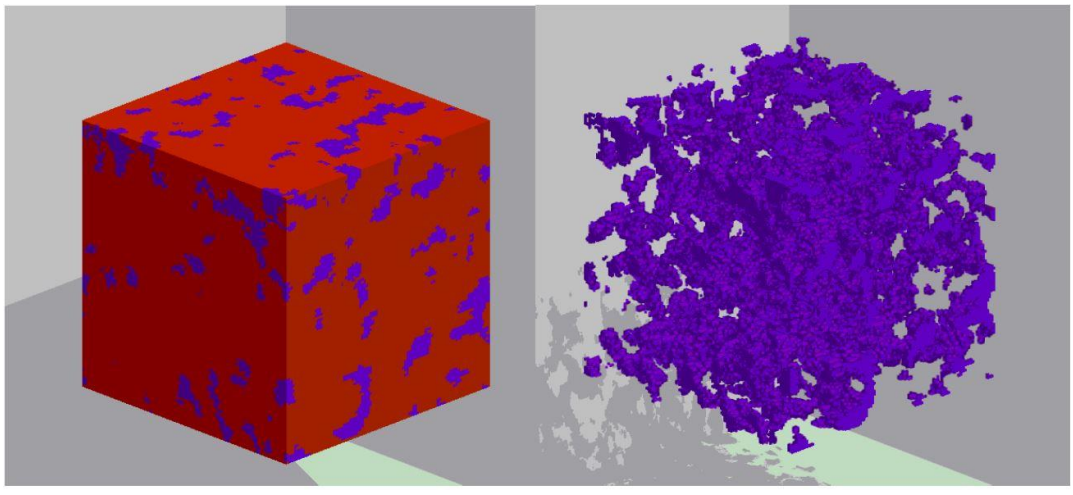

Figure 4-9 Digital Structure and Pore Structure of Sample 5

Table 4-4 Permeability and Porosity Obtained from Digital Cores

Sample	1	2	3	4	5	Average
Permeability (uD)	1.7567	2.01809	1.6688	2.68049	3.62241	2.349298
Porosity (%)	2.37172	2.39542	2.40268	2.43652	2.47996	2.41726

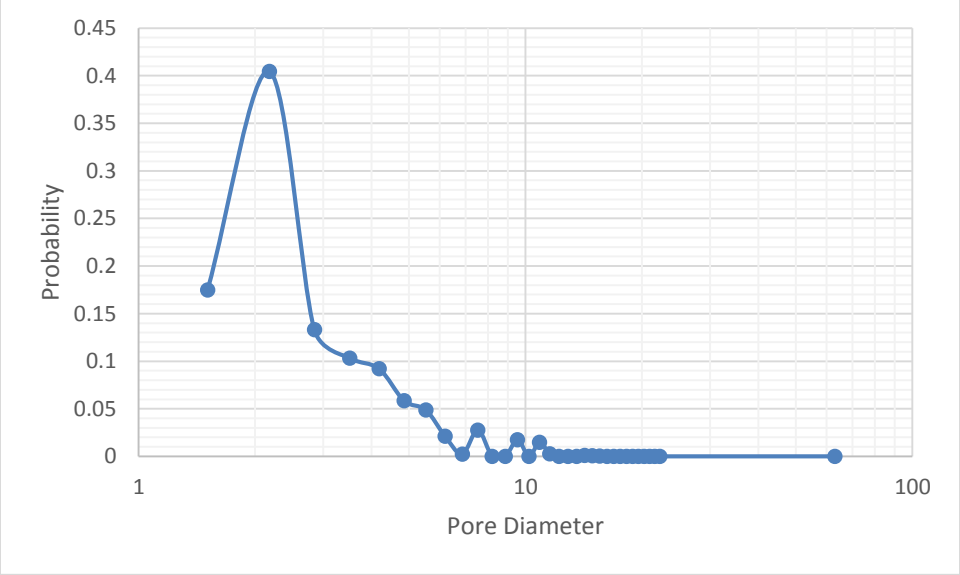

Figure 4-10 Pore-size Distribution of the Digital Core

Both the permeability, porosity and pore-size distribution of the reconstructed core have been calculated using 500^3 voxels, which is equivalent to a few hundreds of cubic nanometers in the presented examples. The permeability and porosity are compared with measured value, shown in Table 4-5, showing that the samples have very close value of the permeability and porosity with the data measured from lab. The comparison of the pore-size distribution is shown in Figure 4-11, and these two curves also shown a very good match. This indicate that the digital core approach is able to capture the pore structure and characteristics of shale formation.

Table 4-5 Permeability and Porosity Comparison between Digital Core and Experiment

	Permeability (uD)	Porosity (%)
Experiment Data	2.75	2.025
Digital Core	2.349298	2.41726

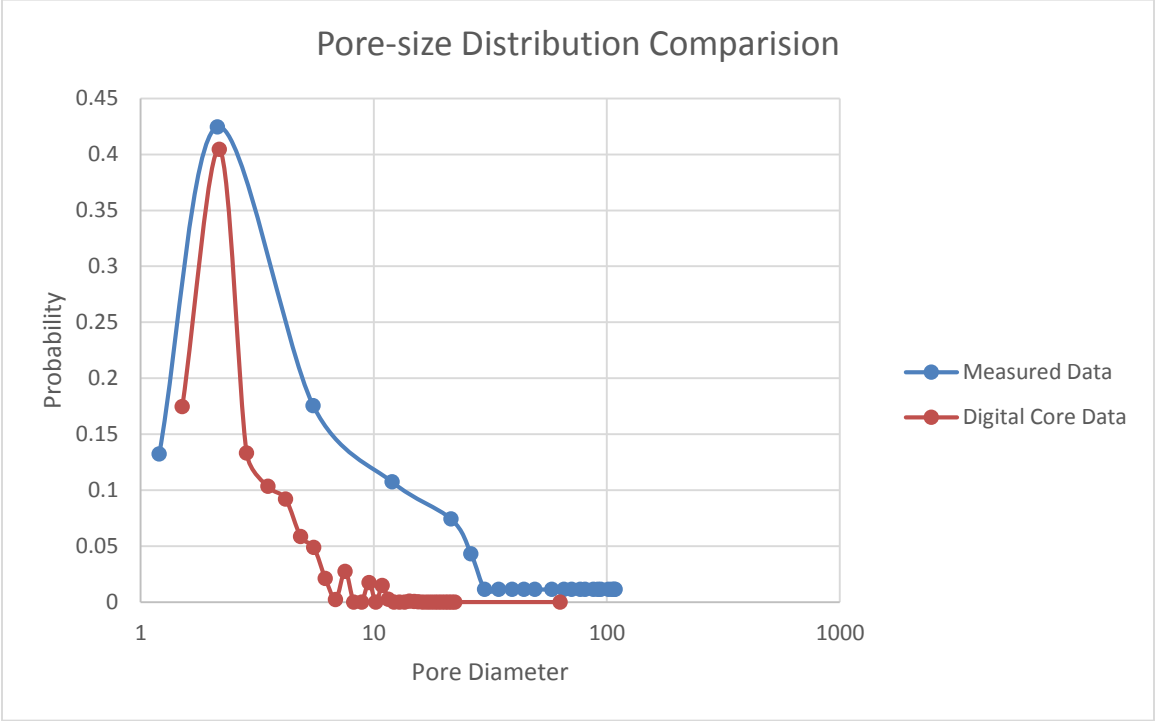

Figure 4-11 Pore-size Distribution Comparison between Digital Core and Experiment

Another observation is a relationship is found between the permeability and porosity of the digital cores. The trend line in Figure 4-12 shows a log-log relationship between these parameters, which

$$\log k = 0.8327 \log \phi + 0.7517,$$

with this equation, we can roughly calculate the permeability of the shale formation by having the porosity. This relationship need to be verified by more data, when we have more samples from the Longmaxi formation.

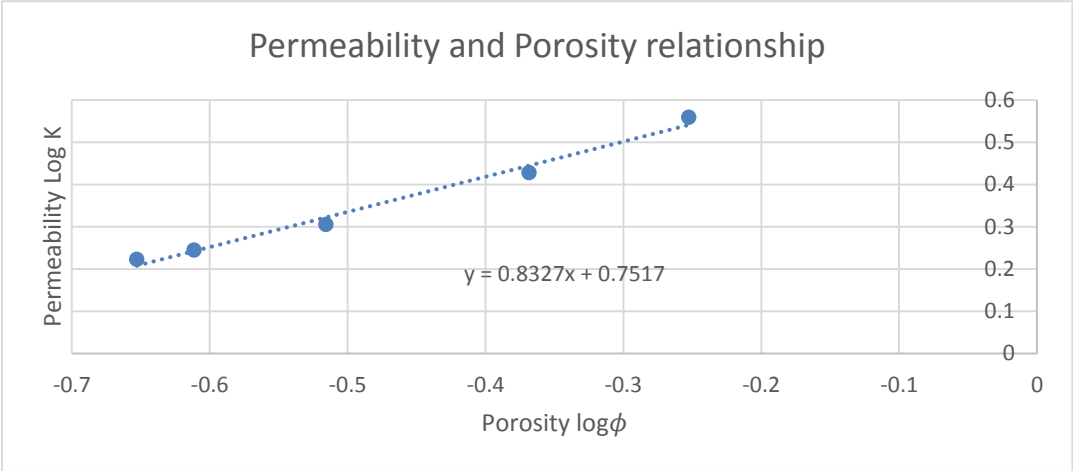

Figure 4-12 Permeability and Porosity Log-log Relationship

CHAPTER 5:Conclusion and Future Work

The goal of this study is to characterize the rock properties in the Lower Silurian Marine Shale, which will help us have a better understanding of the storage and flow mechanisms in shales. In this study, both experimental study and numerical study have been performed. An overview of the major conclusions from this work is summarized below.

1. The results achieved in the laboratory have shown that the Longmaxi Formation has a ultra-low permeability and porosity
2. From the SEM experiment, the Longmaxi shale has a complex nanopore structure and multi-scale pore dimensions; the pore diameters of the Longmaxi shale vary from a few nanometers to hundreds of nanometers.
3. The SEM images also revealed various types of porosity, which can provide considerable pore space for shale gas storage. Also the nanopores plays a very important role in the pore structure of the Longmaxi formation.
4. The digital core is an efficient way to characterize the micropores structure of the shale formation parameters. It is also an efficient way to characterize heterogeneity of shale formation and to understand flow mechanism in shale reservoir.

5. The correlation between the permeability and porosity of the digital cores can provide a fast method to roughly calculate the permeability based on the porosity.

These results are very promising. However, further studies need to be done in the future. First, the constructed 3D digital cores will be used as a numerical simulation foundation for future analysis. More sample is needed to verify both the reliability of digital rock and the correlation between permeability and porosity. Physical reconstruction method, such as FIB/SEM experiment will be conducted in the future. At last, the obtained digital core will be up-scaled to reservoir scale for reservoir simulation

CHAPTER 6:Reference

Ashraf, Ejaz. (1994). Integrated reservoir characterization for the Mazari oil field, Pakistan. Unpublished Master Thesis, Texas A&M University, College Station, USA.

Barrett, E. P., Joyner, L. G., & Halenda, P. P. (1951). The determination of pore volume and area distributions in porous substances. I. Computations from nitrogen isotherms. Journal of the American Chemical society, 73(1), 373-380.

Driskill, B., Walls, J., DeVito, J., & Sinclair, S. W. (2013). Applications of SEM Imaging to Reservoir Characterization in the Eagle Ford Shale, South Texas, USA. Electron Microscopy of Shale Hydrocarbon Reservoirs: AAPG Memoir 102, 102, 115.

Energy Information Administration, Annual Energy Outlook 2013 with projections to 2040, Annual Energy. "Energy Information Administration." United States(2013).

Feast, N., Hackbarth, C., Chen, G., & Huang, Y. (2013, March 26). Pioneering Shale Gas in China: China Sichuan Shale Gas Joint Cooperation Project. International Petroleum Technology Conference. doi:10.2523/16855-MS.

Grader, A., Kalam, M., Toelke, J., Mu, Y., Derzhi, N., Baldwin, C., ... & Yafei, B. S. (2010). A comparative study of digital rock physics and laboratory SCAL evaluations of carbonate cores. In SCA (Vol. 24, p. 2010).

Loucks, R. G., Reed, R. M., Ruppel, S. C., & Jarvie, D. M. (2009). Morphology, genesis, and distribution of nanometer-scale pores in siliceous mudstones of the Mississippian Barnett Shale. Journal of Sedimentary Research, 79(12), 848-861.

Hall, C. E. (1953). Introduction to electron microscopy. Introduction to electron microscopy.

Niblack, W. (1985). An introduction to digital image processing. Strandberg Publishing Company.

Nimmo, J. R. (2004). Porosity and pore size distribution. Encyclopedia of Soils in the Environment, 3, 295-303.

Ning, Yang. (2011). Numerical Investigation of the Cascaded Lattice Boltzmann Method. Unpublished Master Thesis, University of Wyoming, Laramie, USA.

Osborn, S. G., Vengosh, A., Warner, N. R., & Jackson, R. B. (2011). Methane contamination of drinking water accompanying gas-well drilling and hydraulic fracturing. proceedings of the National Academy of Sciences, 108(20), 8172-8176.

Otsu, N. (1975). A threshold selection method from gray-level histograms.Automatica, 11(285-296), 23-27.

Qian, Y. H., d'Humi ères, D., & Lallemand, P. (1992). Lattice BGK models for Navier-Stokes equation. EPL (Europhysics Letters), 17(6), 479.

Sakhaee-Pour, A., & Bryant, S. (2012). Gas permeability of shale. SPE Reservoir Evaluation & Engineering, 15(04), 401-409.

Sondergeld, C. H., Ambrose, R. J., Rai, C. S., & Moncrieff, J. (2010, January). Micro-structural studies of gas shales. In SPE Unconventional Gas Conference. Society of Petroleum Engineers.

Wang, Chenchen. (2012). Construction Theory and Method of Dual Pore Network Model in Carbonate Media. Unpublished doctoral dissertation, China University of Petroleum, Qingdao, China.

Wei, Chenji. (2013). Formation evaluation and numerical modeling on hydraulic fracturing for an emerging marine shale gas reservoir. Unpublished doctoral dissertation, University of Wyoming, Laramie, USA.

Wei, C., & Qin, G. (2013, November 11). Microstructure Characterization for a Shale Gas Reservoir by Combining Visualization Technique and Physical Measurement. Society of Petroleum Engineers. doi:10.2118/167610-MS.

Yao, J., Wang, C., Yang, Y., Hu, R., & Wang, X. (2013). The construction of carbonate digital rock with hybrid superposition method. Journal of Petroleum Science and Engineering, 110, 263-267.

Zhang, H., Bai, B., Song, K., & Elgmati, M. M. (2012, January 1). Shale Gas Hydraulic Flow Unit Identification Based on SEM-FIB Tomography. Society of Petroleum Engineers. doi:10.2118/160143-MS.